

Asymmetry-Based Quantum Backaction Suppression in Quadratic Optomechanics

Vincent Dumont,^{1,*} Hoi-Kwan Lau²,³ Aashish A. Clerk,³ and Jack C. Sankey¹

¹*Department of Physics, McGill University, Montréal, Québec H3A 2T8, Canada*

²*Department of Physics, Simon Fraser University, Burnaby, British Columbia V5A 1S6, Canada*

³*Pritzker School of Molecular Engineering, University of Chicago, Chicago, Illinois 60637, USA*

 (Received 15 March 2022; revised 17 May 2022; accepted 24 June 2022; published 4 August 2022)

As the field of optomechanics advances, quadratic dispersive coupling (QDC) represents an increasingly feasible path toward qualitatively new functionality. However, the leading QDC geometries generate linear *dissipative* coupling and an associated quantum radiation force noise that is detrimental to QDC applications. Here, we propose a simple geometry that dramatically reduces this noise *without* altering the QDC strength. We identify optimal regimes of operation, and discuss advantages within the examples of optical levitation and nondestructive phonon measurement.

DOI: [10.1103/PhysRevLett.129.063604](https://doi.org/10.1103/PhysRevLett.129.063604)

Introduction.—The field of optomechanics [1] explores the forces exerted by light, increasingly accessing the quantum regime with an eye toward sensing, information, and fundamental tests of macroscopic quantum motion. To date, the vast majority of experimental breakthroughs—e.g., room-temperature broadband squeezing [2], measurement near the Heisenberg limit or below the standard quantum limit [3,4], quantum transduction [5], and generation of quantum motion [6]—have been achieved in systems having so-called linear dispersive coupling (LDC), wherein an optical resonance frequency depends linearly on mechanical displacement. As the field advances, systems exhibiting purely quadratic dispersive coupling (QDC), wherein the optical frequency depends on the displacement *squared*, promise another wave of applications that are qualitatively different than can be achieved with LDC, including quantum nondemolition (QND) readout of the phonon number [7–13] or shot noise [14], generation of exotic and non-Gaussian quantum states [15–19], nonreciprocal photon control [20], phonon blockade [21], two-phonon cooling [16,22], mechanical squeezing [23], and stable center-of-mass [24,25] or torsional [26] optical traps for geometry tuned [27], and ultrahigh- Q [25,28] mechanical systems. Currently, the number of LDC applications far outstrips that of QDC, which is not surprising: LDC is the leading-order effect most easily realized experimentally, and so it is sensible to pursue LDC applications while developing the techniques and understanding required for higher order coupling. As linear

applications transition from proof-of-concept demonstrations to engineering, the forefront of fundamental discovery will shift to new optomechanical interactions, with a natural next step being QDC.

QDC optomechanical systems can mostly be mapped onto a canonical “membrane-in-the-middle” (MIM) [7,9] paradigm, wherein a partially reflective, flexible membrane splits a Fabry-Perot cavity into two identical subcavities, such that their LDC mutually cancels, producing pure QDC to leading order. This configuration has been successfully realized with a membrane in a macroscopic [7] or microscopic [29] cavity, on-chip [30,31] (and with qubits [32,33]), levitated [34], and with atomic clouds [35]. Notably, extraordinarily sensitive applications such as quadratic cooling [34], phonon number sensitive measurements [32], and mechanical energy squeezing [33] are now viable.

Importantly, QDC is always accompanied by a linear *dissipative* coupling [36–43], introducing associated quantum radiation force noise (QRFN) [10,44,45] that restricts possibilities, especially in the quantum regime [10,44,45]. Gaining control over this fundamentally quantum source of noise is therefore of paramount importance.

Here we propose an optomechanical geometry that dramatically reduces QRFN *without* compromising the strength of QDC. Specifically, our system exploits two nonidentical subcavities, a situation readily realized in the canonical system by displacing the membrane. A previous classical wave analysis showed that a membrane displaced towards the back mirror in an idealized “single-port” system (one in which optical loss is entirely through the input mirror) can exhibit reduced linear coupling between displacement and the cavity’s total dissipation [46], suggesting (without proof) the possibility of suppressed QRFN when there are no internal losses. Here, we present the requisite full quantum analysis to prove this conjecture, and

Published by the American Physical Society under the terms of the Creative Commons Attribution 4.0 International license. Further distribution of this work must maintain attribution to the author(s) and the published article’s title, journal citation, and DOI.

quantify its ultimate limits in the presence of losses. In the ideal single-port case, QRFN can indeed be reduced by many orders of magnitude via subcavity asymmetry (meaning previous theoretical limits [10,44] are not fundamental); and with finite internal loss, our analysis identifies the optimal asymmetry that minimizes QRFN, notably still achieving several orders of magnitude reduction with realistic device parameters. We then discuss how this enables cavity-assisted optical levitation with noise below that of free-space traps (or MIM systems) and similarly improves QND phonon number measurements.

Quantum model.—For illustrative purposes, we now focus on the membrane-cavity geometry drawn in Fig. 1(a), stressing that this serves as a canonical system representing all such QDC systems; similar results and general expressions are provided in the Supplemental Material [47]. The setup comprises a cavity of length L partitioned into two subcavities by a membrane with (field) transmission $|t_m| \ll 1$. Including the membrane’s displacement operator \hat{x} , the lengths of the subcavities are $L_1 + \hat{x}$ and $L_2 - \hat{x}$, where L_1 and $L_2 \equiv L - L_1$ are chosen such that the subcavities are degenerate at frequency $\omega_0 = N_1\pi c/L_1 = N_2\pi c/L_2$ for integers N_1 and N_2 . The Hamiltonian of the photonic fields $\hat{H}_{\text{opt}} = \hat{H}_1 + \hat{H}_2 + \hat{H}_c$, where, to leading order in \hat{x} , the

subcavity energies $\hat{H}_j = \hbar[\omega_0 + \hat{x}(-1)^j\omega_0/L_j]\hat{a}_j^\dagger\hat{a}_j$ for $j = 1, 2$, and \hat{a}_j is the photon annihilator. Membrane transmission couples the subcavities via $\hat{H}_c = -\hbar J(\hat{a}_1^\dagger\hat{a}_2 + \hat{a}_2^\dagger\hat{a}_1)$ at a rate $J = c|t_m|/(2\sqrt{L_1L_2})$ [47].

In contrast to a MIM setup, to obtain purely QDC, the mean position of the membrane needs to be displaced to a “quadratic point” [Fig. 1(b)]. We first define the membrane’s quantum motion \hat{z} around the classical displacement Δx , i.e., $\hat{x} \equiv \Delta x + \hat{z}$ where $\Delta x \ll L_j$, such that the optical Hamiltonian can be generally rewritten as

$$\hat{H}_{\text{opt}} = \hat{H}_p + \hat{z}\hat{F}_{\text{opt}}, \quad (1)$$

where \hat{H}_p involves only photonic fields, and

$$\hat{F}_{\text{opt}} = \hbar\omega_0(\hat{a}_1^\dagger\hat{a}_1/L_1 - \hat{a}_2^\dagger\hat{a}_2/L_2) \quad (2)$$

is the radiation force [52]. At any Δx , the eigenmodes of \hat{H}_p can be expressed succinctly as

$$\hat{a}_\pm(\Delta x) = \cos(\theta_\pm)\hat{a}_1 + \sin(\theta_\pm)\hat{a}_2, \quad (3)$$

where the amplitudes satisfy $\cot(2\theta_\pm) = \pm L\omega_0\Delta x/\sqrt{L_1L_2}c|t_m|$. In terms of \hat{a}_\pm , $\hat{H}_p = \hbar\omega_+\hat{a}_+^\dagger\hat{a}_+ + \hbar\omega_-\hat{a}_-^\dagger\hat{a}_- \equiv \hat{H}_+ + \hat{H}_-$, with eigenfrequencies

$$\omega_\pm = \omega_0 + \frac{(L_2 - L_1)\omega_0\Delta x}{2L_1L_2} \mp \sqrt{\left(\frac{L\omega_0\Delta x}{2L_1L_2}\right)^2 + J^2}, \quad (4)$$

while $\hat{F}_{\text{opt}} = h_+\hat{a}_+^\dagger\hat{a}_+ + h_c(\hat{a}_+^\dagger\hat{a}_- + \hat{a}_-^\dagger\hat{a}_+) + h_-\hat{a}_-^\dagger\hat{a}_-$, with coefficients h_+ , h_c , h_- depending on the eigenmode composition (and thus Δx).

The dispersive coupling associated with the \pm modes is generally linear (i.e., the adiabatic eigenfrequencies depend linearly on position to leading order), with exceptions at membrane displacements

$$\Delta x_\pm = \pm \frac{c|t_m|L_1 - L_2}{2\omega_0 L}, \quad (5)$$

where the frequency of one eigenmode exhibits QDC to leading order in \hat{z} (i.e., $h_\pm = 0$ at Δx_\pm). For simplicity, we focus on Δx_+ hereafter, since the key results are identical at Δx_- . The leading *coherent* optomechanical effect on \hat{a}_+ is tunnelling with \hat{a}_- , but, due to the separation of eigenfrequencies [Eq. (4)], \hat{a}_- can be adiabatically eliminated—an approximation that does not hold if the frequency splitting $2J$ becomes comparable to the mechanical frequency Ω_m [13]—and the \hat{a}_+ dynamics are governed by pure QDC via

$$\hat{H}_+ = \hbar\left(\omega_+ + \frac{2\omega_0^2}{c|t_m|L}\hat{z}^2\right)\hat{a}_+^\dagger\hat{a}_+. \quad (6)$$

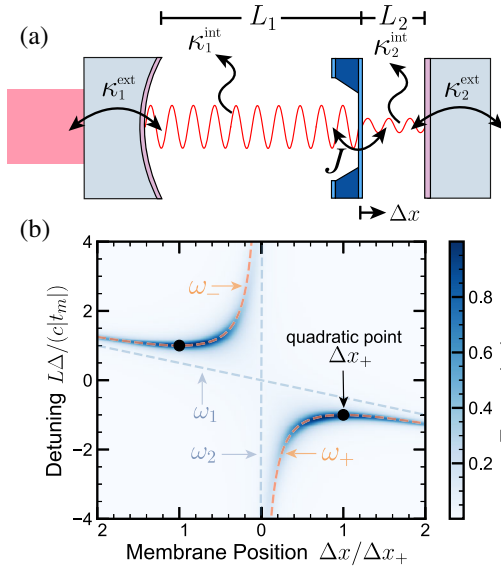


FIG. 1. Membrane-cavity system. (a) Fabry-Perot cavity asymmetrically split by a membrane (blue) of transmission $|t_m|$ into two subcavities of lengths L_j . The subcavities are coupled to each other through the membrane at rate J . Drive and detection are conducted through external coupling at rates κ_j^{ext} , while photons are lost at rates κ_j^{int} . (b) Cavity transmission versus membrane position Δx and drive detuning $\Delta \equiv \omega_{\text{in}} - \omega_0$. In this example, $|t_m|^2 = 7 \times 10^4$ ppm, $|t_1|^2 = 6 \times 10^4$ ppm, $|t_2|^2 = 4 \times 10^4$ ppm, and $L_1/L_2 = 10^3$. Grey dashed lines show the uncoupled ($J = 0$) subcavity frequencies $\omega_{\text{in}} = \omega_j \equiv \omega_0[1 + (-1)^j\Delta x/L_j]$; orange dashed lines show eigenfrequencies ω_\pm .

Importantly, this shows that the overall QDC strength is determined only by the total cavity length L , with no dependence on L_j , in agreement with classical wave analysis [46]: at a quadratic point, the subcavity circulating powers are balanced, applying no net force (otherwise there would necessarily be LDC), and the power imbalance arising from displacing the membrane is then determined solely by the membrane scattering coefficients and incident field phases, which remain unchanged when adjusting L_j by an integer number of half-wavelengths.

Dissipative force noise.—The effective adiabatic Hamiltonian in Eq. (6) is purely quadratic in \hat{z} , but coupling to an external environment generates linear dissipative backaction. The external coupling and internal loss rates are, respectively,

$$\kappa_j^{\text{ext}} = c|t_j|^2/(2L_j), \quad \kappa_j^{\text{int}} = c\mathcal{L}_j/(2L_j), \quad (7)$$

where t_j is the end-mirror field transmission, and \mathcal{L}_j is the round-trip photon loss fraction for subcavity j , such that the total round-trip loss $\mathcal{T}_j = |t_j|^2 + \mathcal{L}_j$. The associated QRFN power spectral density $S_{FF}(\omega) = \int e^{i\omega t} \langle \delta\hat{F}(t)\delta\hat{F}(0) \rangle dt$ (where $\delta\hat{F} \equiv \hat{F}_{\text{opt}} - \langle \hat{F}_{\text{opt}} \rangle$) is the optical force fluctuation [53]), quantified in different limits below.

Ideal single-port cavity.—To illustrate the fundamental potential for improvement, we first consider a single-port cavity ($\kappa_2^{\text{int}} = \kappa_2^{\text{ext}} = 0$). In the presence of drive, $S_{FF}(\omega)$ can be calculated from linearized Heisenberg-Langevin equations of motion [53]. If \hat{a}_+ mode is driven through mirror 1 at frequency ω_{in} , the QRFN spectral density becomes [47]

$$S_{FF}(\omega) = \hbar^2 |\bar{a}_+|^2 \kappa_1 L \left(\frac{\omega_0}{L_1 L_2} \right)^2 \times \frac{|L_2 \tilde{\chi}_{11}(\omega) + iL_1 J \chi_2^*(0) \tilde{\chi}_{21}(\omega)|^2}{|\sqrt{L_1} + i\sqrt{L_2} J \chi_2(0)|^2}, \quad (8)$$

where $|\bar{a}_+|^2$ is the mean photon number, $\kappa_j \equiv \kappa_j^{\text{ext}} + \kappa_j^{\text{int}}$ is the total loss rate of subcavity j , $\chi_j(\omega) = [-i(\omega_{\text{in}} - \omega_0 + (-1)^{j+1} \omega_0 \Delta x_+ / L_j + \omega) + \kappa_j/2]^{-1}$ is the susceptibility, and $\tilde{\chi}_{lm}$ are matrix elements of the eigenmode susceptibility

$$\tilde{\chi}(\omega) = \frac{1}{\chi_1^{-1}(\omega)\chi_2^{-1}(\omega) + J^2} \begin{pmatrix} \chi_2^{-1}(\omega) & iJ \\ iJ & \chi_1^{-1}(\omega) \end{pmatrix}. \quad (9)$$

In the “large-gap” limit $2c|t_m|/L \gg \kappa_1, \kappa_2, |\omega|$, and when the drive is resonant with \hat{a}_+ ($\omega_{\text{in}} = \omega_+$),

$$S_{FF}(\omega) \rightarrow \left(\frac{2L_2}{L} \right)^2 \frac{\hbar^2 |\bar{a}_+|^2 \omega_0^2}{c^2 |t_m|^2} \frac{\omega^2 \kappa_+}{\omega^2 + \kappa_+^2/4}, \quad (10)$$

where the \hat{a}_+ decay rate is $\kappa_+(\Delta x_+) = \kappa_1 L_1/L$. The frequency dependence arises from a combination of the

cavity mode’s “low-pass” response (bandwidth κ_+) and destructive interference with the promptly reflected drive [36] at low frequencies. Inspecting the first factor, the fundamental advantage of our setup becomes clear: when the membrane is positioned near the back mirror, ($L_2 \ll L_1 \approx L$), QRFN is suppressed by a factor $(2L_2/L)^2$. Here, the backaction is entirely due to the cavity mode’s *total* dissipative coupling $\partial_x \kappa_+$ [36,44] leaking information about membrane position. Classically [46,47], the gradient $\partial_x \kappa_+$ is maximal with the membrane near the front mirror (the resulting “compound input mirror” has an overall transmission modulated by membrane motion) and minimal when the membrane is near the back mirror, which is already so reflective that the membrane does not impact κ_+ . In a centimeter-scale cavity with wavelength-scale membrane-mirror separation, this suppression factor can reach $(2L_2/L)^2 \sim 10^{-8}$ relative to a MIM system ($L_2 = L/2$). We stress that this is achieved while the quadratic coupling in Eq. (6) remains unchanged. Notably, this simple result illustrates that the “standard quantum limit” [10] for quadratic readout in these MIM systems, which persists even in ideal, lossless, single-port systems [44], is not fundamental.

Lossy cavity.—Including losses via \mathcal{L}_1 and \mathcal{T}_2 [47],

$$S_{FF}(\omega) = \frac{\hbar^2 |\bar{a}_+|^2 \omega_0^2 L_2}{c^2 |t_m|^2} \frac{4L_1 \kappa_- \omega^2 + L \kappa_+^2 \kappa_2}{L^2 (\omega^2 + \kappa_+^2/4)}, \quad (11)$$

where the eigenmode dissipation rates are $\kappa_+ = \kappa_1 L_1/L + \kappa_2 L_2/L$ and $\kappa_- = \kappa_1 L_2/L + \kappa_2 L_1/L$. Compared to Eq. (10), the loss ports have introduced noise that is not suppressed as $\omega \rightarrow 0$, since those ports have no reflection with which to interfere. Since membrane motion linearly modulates the subcavity amplitudes [via Eq. (3)], this term can be thought of as the backaction associated with position information encoded in the relative power escaping the two subcavities. Additionally, because κ_2 [part of κ_- in Eq. (11)] scales inversely with L_2 , QRFN cannot be suppressed indefinitely by shrinking the second subcavity. Instead, $S_{FF}(\Omega_M)$ reaches a minimum at an optimal first subcavity length [47]

$$L_{1,\text{min}} = \frac{\mathcal{T}_1}{\mathcal{T}_1 + \mathcal{T}_2} L. \quad (12)$$

One might have guessed this location, since it balances the subcavity loss rates ($\kappa_1 = \kappa_2$), such that the total loss gradient $\partial_x \kappa_+ = 0$ (κ_+ is always a weighted sum of κ_1 and κ_2), thereby preventing additional position information (beyond that encoded in the relative subcavity powers) from leaving the cavity. Finally, at quadratic points near $L_{1,\text{min}}$, the QRFN at mechanical frequency Ω_m becomes

$$S_{FF}^{\text{min}}(\Omega_m) = 2 \frac{\hbar^2 |\bar{a}_+|^2 \omega_0^2}{cL |t_m|^2} \mathcal{T}_2 \frac{1 + 4\mathcal{B}\Omega_m^2/\kappa_+^2}{1 + 4\Omega_m^2/\kappa_+^2}, \quad (13)$$

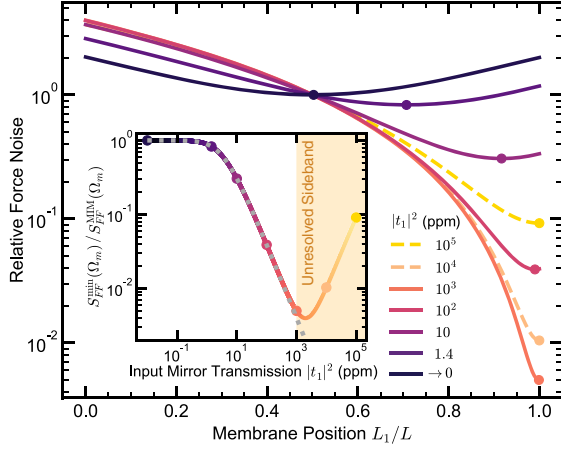


FIG. 2. $S_{FF}(\Omega_m)$ relative to MIM, for a “typical” canonical setup: cavity length $L = 10$ cm, transmissions $|t_m|^2 = 10^4$ ppm [54] and $|t_2|^2 = 0$, losses $\mathcal{L}_j = 1$ ppm [55,56], and mechanical frequency $\Omega_m = 2\pi \times 240$ kHz, with a wide range of input transmissions $|t_1|^2$. The solid (dashed) curves are in the resolved (unresolved) sideband regime, and markers indicate optimal membrane position [Eq. (12)]. For $|t_1|^2 = 10^3$ ppm, the force noise can be reduced by a factor of 250. Inset: optimal reduction of force noise. The shading indicates the unresolved sideband regime, and the dotted line corresponds to the resolved-sideband approximation [Eq. (16)].

where $\mathcal{B} \equiv \mathcal{T}_1/(\mathcal{T}_1 + \mathcal{T}_2)$. To get a sense of potential improvement in laser-driven cavities with dielectric mirrors, e.g., Fig. 2 shows these results for a variety of experimentally feasible parameters. The dashed line shows the predicted optimal suppression in a modified form of the “resolved-sideband” regime [47] $\Omega_m \gg \kappa_+ \sqrt{L\kappa_-/4L_1\kappa_-}$ wherein the above expression simplifies to

$$S_{FF}(\Omega_m) \rightarrow 4 \frac{\hbar^2 |\bar{a}_+|^2 \omega_0^2 L_1 L_2}{c^2 |t_m|^2 L^2} \kappa_- \quad (14)$$

with an optimal value

$$S_{FF}^{\min}(\Omega_m) \rightarrow 2 \frac{\hbar^2 |\bar{a}_+|^2 \omega_0^2}{cL |t_m|^2} \frac{\mathcal{T}_1 \mathcal{T}_2}{\mathcal{T}_1 + \mathcal{T}_2}, \quad (15)$$

and a noise suppression (relative to MIM)

$$\frac{S_{FF}^{\min}(\Omega_m)}{S_{FF}^{\text{MIM}}(\Omega_m)} = 4 \frac{\mathcal{T}_1 \mathcal{T}_2}{(\mathcal{T}_1 + \mathcal{T}_2)^2} \rightarrow 4 \frac{\mathcal{T}_2}{\mathcal{T}_1}, \quad (16)$$

where the last step is in the near-single-port limit $\mathcal{T}_1 \gg \mathcal{T}_2$. Note this result highlights that QRFN cannot be estimated from the total loss gradient $\partial_x \kappa_+$, which is why an ideal, balanced MIM system exhibiting $\partial_x \kappa_+ = 0$ has such a strict limit for QND measurement [10]. As shown in the inset, our scheme is most advantageous in the single-port limit (larger $|t_1|^2$), with diminishing returns in the deeply

unresolved sideband regime. Importantly, QRFN for these “typical” parameters can be suppressed by more than 2 orders of magnitude (and beyond with larger L and/or Ω_m).

Equations (13) and (16) comprise our main result: QRFN can be significantly suppressed by introducing asymmetry to the underlying subcavity modes, and without reducing the QDC strength. Note this suppression ultimately depends on how “single-port” and “resolved-sideband” the cavity is, and similar reduction can be achieved with very different overall losses. This result directly benefits all QDC applications, and we now discuss the illustrative examples of levitation and QND measurement.

Optical levitation.—By placing a minimally supported reflector at a quadratic point, the reflector’s motion can be optically trapped. For a resolved-sideband cavity driven at $\omega_{\text{in}} = \omega_+ \approx \omega_0$, the dispersive optical spring constant at Δx_+ is $\hbar \omega'' |\bar{a}_+|^2 \approx (8/|t_m|)(\omega_{\text{in}} \bar{P}_{\text{circ}}/c^2)$, with $\omega''/2 = 2\omega_0^2/c|t_m|L$ taken from Eq. (6). This spring constant is identical to that of a standing wave in free space for the same circulating power \bar{P}_{circ} . However, a free space trap’s QRFN $S_{FF}^{\text{FS}} \approx 8\hbar\omega_{\text{in}} \bar{P}_{\text{in}}/c^2$, meaning our optimal membrane-cavity system has a relative force noise (from Eq. (15))

$$\frac{S_{FF}^{\min}(\Omega_m)}{S_{FF}^{\text{FS}}} = \frac{1}{2|t_m|^2} \frac{\mathcal{T}_1 \mathcal{T}_2}{\mathcal{T}_1 + \mathcal{T}_2} \rightarrow \frac{\mathcal{T}_2}{2|t_m|^2}, \quad (17)$$

with the last expression in the nearly single-port limit. Stated briefly, as long as most of the back-cavity light leaves through the membrane (i.e., $|t_m|^2 \gg \mathcal{T}_2$), QRFN can be significantly suppressed relative to free space (or MIM). Furthermore, \bar{P}_{circ} in a cavity system is achieved with significantly less input power, making it far easier to realize a quantum-limited light source that actually reaches this QRFN limit. This also comes without the instabilities associated with a LDC spring (e.g., antidamping [1]).

QND phonon measurement.—In the resolved-sideband regime, QDC measures time-averaged mechanical energy, enabling quantum nondemolition (QND) readout of the phonon number [7,9,47]. This is traditionally proposed assuming a near-single-port cavity, which benefits from increased collection efficiency $\sim |t_1|^2/(\mathcal{T}_1 + \mathcal{T}_2)$ and other technical advantages. We quantify the quantum-limited performance of such measurements with the ratio of measurement rate Γ_{meas} to backaction rate $\Gamma_{\text{BA},n}$ [10], a figure of merit that exceeds one when it is possible to resolve phonon number state n before QRFN causes a jump. For our setup, when \hat{a}_+ is driven on resonance, this ratio becomes (again assuming large-gap and modified resolved-sideband limits) [47]

$$\frac{\Gamma_{\text{meas}}}{\Gamma_{\text{BA},n}} = \frac{64}{2n+1} \left[\frac{g_1 g_2}{\kappa_- \kappa_+} \right] \left(\frac{\kappa_1^{\text{ext}} L_1}{\kappa_+ L} \right) \equiv \frac{x_{\text{ZPF}}^2}{x_{\text{res}}^2}, \quad (18)$$

where $g_j = \omega_0 x_{\text{ZPF}}/L_j$ is the single-photon optomechanical coupling rate for subcavity j , and $x_{\text{ZPF}} = \sqrt{\hbar/2m\Omega_m}$ is the zero-point fluctuation of the membrane (mass m).

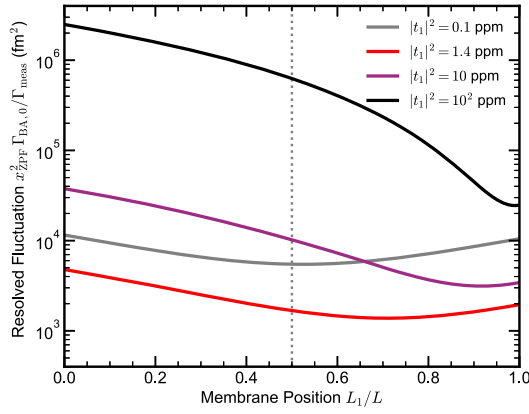


FIG. 3. Resolvable fluctuation x_{res}^2 for QND measurement of the mechanical ground state ($n = 0$). Our scheme exhibits clear advantage for a wide range of front mirror transmission $|t_1|^2$ (black and purple), achieving a factor of 25 improvement over the MIM configuration in a near-single-port system with $|t_1|^2 = 10^2$ ppm (black), and provides additional improvement when optimizing $|t_1|^2$ [red; see Eq. (19)]. Further reducing $|t_1|^2$ provides no benefit due to reduced collection efficiency. The system parameters are $\mathcal{L}_1 = \mathcal{L}_2 = 1$ ppm, $|t_2|^2 = 0$ ppm (loss-limited Bragg stack), $|t_m|^2 = 10^4$ ppm, and $L = 10$ cm, $\omega_{\text{in}} = \omega_+$ in the resolved-sideband regime. The dotted vertical line indicates $L_1 = L/2$. The y axis indicates the minimal zero-point variance x_{ZPF}^2 required to resolve the ground state.

We define a “resolvable variance” x_{res}^2 —the value of x_{ZPF}^2 needed to achieve unity $\Gamma_{\text{meas}}/\Gamma_{\text{BA},n}$ —as our figure of merit because it solely depends on the optical properties of our system, unlike $\Gamma_{\text{meas}}/\Gamma_{\text{BA},n}$. The factor $\kappa_1^{\text{ext}}L_1/\kappa_+L$ captures the cavity mode’s input coupling efficiency, while the square root of the factor $g_1g_2/\kappa_-\kappa_+$ characterizes single-photon strong coupling for asymmetric systems.

For single-port approaches, Eq. (18) yields dramatic improvements over the MIM approach, as shown in Fig. 3; this is entirely due to the force noise suppression in Eq. (16), since $\Gamma_{\text{BA},n} \propto S_{FF}$ and the quadratic coupling strength is independent of L_1 . In systems operating away from the single-port regime, our analysis identifies an optimal input mirror transmission [47]

$$|t_1|_{\text{opt}}^2 = \sqrt{\mathcal{L}_1(\mathcal{L}_1 + \mathcal{L}_2 + |t_2|^2)}. \quad (19)$$

This further improves x_{res}^2 as shown by the red curve in Fig. 3.

Summary.—We propose an optomechanical setup that dramatically reduces quantum radiation force noise without affecting the quadratic dispersive coupling strength. For the canonical membrane-cavity geometry, this is implemented by simply relocating the membrane toward the mirror with higher reflectivity. Our quantum analysis identifies optimal configurations, and we demonstrate its advantage in optical levitation and nondemolition phonon number

measurement. Owing to its ease of implementation and the universal desire to control quantum noise, we expect this work to immediately impact all optomechanical experiments aiming to utilize quadratic dispersive coupling.

We thank Simon Bernard, Lilian Childress, Bill Coish, Zoé McIntyre, Christoph Reinhardt, and Yariv Yanay for fruitful discussions. V. D. acknowledges financial support from FRQNT-B2 Scholarship and McGill Schulich Graduate Fellowship. H.-K. L. acknowledges support from Canada Research Chairs. A. C. acknowledges support from the Simons Foundation under a Simons Investigator Award. J. C. S. acknowledges relevant support from the Natural Sciences and Engineering Research Council of Canada (NSERC RGPIN 2018-05635), Canada Research Chairs (235060), Institut Transdisciplinaire d’Information Quantique (INTRIQ), and the Centre for the Physics of Materials (CPM) at McGill.

*vincent.dumont@mail.mcgill.ca

- [1] M. Aspelmeyer, T. J. Kippenberg, and F. Marquardt, Cavity optomechanics, *Rev. Mod. Phys.* **86**, 1391 (2014).
- [2] N. Aggarwal, T. J. Cullen, J. Cripe, G. D. Cole, R. Lanza, A. Libson, D. Follman, P. Heu, T. Corbitt, and N. Mavalvala, Room-temperature optomechanical squeezing, *Nat. Phys.* **16**, 784 (2020).
- [3] D. Mason, J. Chen, M. Rossi, Y. Tsaturyan, and A. Schliesser, Continuous force and displacement measurement below the standard quantum limit, *Nat. Phys.* **15**, 745 (2019).
- [4] H. Yu, L. McCuller, M. Tse, N. Kijbunchoo, L. Barsotti, and N. Mavalvala, Quantum correlations between light and the kilogram-mass mirrors of LIGO, *Nature (London)* **583**, 43 (2020).
- [5] Y. Chu and S. Gröblacher, A perspective on hybrid quantum opto- And electromechanical systems, *Appl. Phys. Lett.* **117**, 150503 (2020).
- [6] S. Barzanjeh, A. Xuereb, S. Gröblacher, M. Paternostro, C. A. Regal, and E. M. Weig, Optomechanics for quantum technologies, *Nat. Phys.* **18**, 15 (2022).
- [7] J. Thompson, B. Zwickl, A. Jayich, F. Marquardt, S. Girvin, and J. Harris, Strong dispersive coupling of a high-finesse cavity to a micromechanical membrane, *Nature (London)* **452**, 72 (2008).
- [8] M. Bhattacharya, H. Uys, and P. Meystre, Optomechanical trapping and cooling of partially reflective mirrors, *Phys. Rev. A* **77**, 033819 (2008).
- [9] A. Jayich, J. Sankey, B. Zwickl, C. Yang, J. Thompson, S. Girvin, A. A. Clerk, F. Marquardt, and J. Harris, Dispersive optomechanics: A membrane inside a cavity, *New J. Phys.* **10**, 095008 (2008).
- [10] H. Miao, S. Danilishin, T. Corbitt, and Y. Chen, Standard Quantum Limit for Probing Mechanical Energy Quantization, *Phys. Rev. Lett.* **103**, 100402 (2009).
- [11] L. Dellantonio, O. Kyriienko, F. Marquardt, and A. S. Sørensen, Quantum nondemolition measurement of mechanical motion quanta, *Nat. Commun.* **9**, 3621 (2018).

- [12] B. D. Hauer, A. Metelmann, and J. P. Davis, Phonon quantum nondemolition measurements in nonlinearly coupled optomechanical cavities, *Phys. Rev. A* **98**, 043804 (2018).
- [13] M. Ludwig, A. H. Safavi-Naeini, O. Painter, and F. Marquardt, Enhanced Quantum Nonlinearities in a Two-Mode Optomechanical System, *Phys. Rev. Lett.* **109**, 063601 (2012).
- [14] A. A. Clerk, F. Marquardt, and J. G. E. Harris, Quantum Measurement of Phonon Shot Noise, *Phys. Rev. Lett.* **104**, 213603 (2010).
- [15] M. R. Vanner, Selective Linear or Quadratic Optomechanical Coupling via Measurement, *Phys. Rev. X* **1**, 021011 (2011).
- [16] A. Nunnenkamp, K. Børkje, J. G. E. Harris, and S. M. Girvin, Cooling and squeezing via quadratic optomechanical coupling, *Phys. Rev. A* **82**, 021806(R) (2010).
- [17] H. Xie, X. Shang, C.-G. Liao, Z.-H. Chen, and X.-M. Lin, Macroscopic superposition states of a mechanical oscillator in an optomechanical system with quadratic coupling, *Phys. Rev. A* **100**, 033803 (2019).
- [18] M. Brunelli, O. Houhou, D. W. Moore, A. Nunnenkamp, M. Paternostro, and A. Ferraro, Unconditional preparation of nonclassical states via linear-and-quadratic optomechanics, *Phys. Rev. A* **98**, 063801 (2018).
- [19] M. Brunelli and O. Houhou, Linear and quadratic reservoir engineering of non-gaussian states, *Phys. Rev. A* **100**, 013831 (2019).
- [20] X. Xu, Y. Zhao, H. Wang, H. Jing, and A. Chen, Quantum nonreciprocity in quadratic optomechanics, *Photonics Res.* **8**, 143 (2020).
- [21] H. Xie, C.-G. Liao, X. Shang, M.-Y. Ye, and X.-M. Lin, Phonon blockade in a quadratically coupled optomechanical system, *Phys. Rev. A* **96**, 013861 (2017).
- [22] S. Chiavazzo, A. S. Sørensen, O. Kyriienko, and L. Dellantonio, Quantum manipulation of a two-level mechanical system, [arXiv:2101.01750](https://arxiv.org/abs/2101.01750).
- [23] M. Asjad, G. S. Agarwal, M. S. Kim, P. Tombesi, G. Di Giuseppe, and D. Vitali, Robust stationary mechanical squeezing in a kicked quadratic optomechanical system, *Phys. Rev. A* **89**, 023849 (2014).
- [24] D. Chang, C. Regal, S. Papp, D. Wilson, J. Ye, O. Painter, H. Kimble, and P. Zoller, Cavity opto-mechanics using an optically levitated nanosphere, *Proc. Natl. Acad. Sci. U.S.A.* **107**, 1005 (2010).
- [25] D. Chang, K.-K. Ni, O. Painter, and H. Kimble, Ultrahigh- q mechanical oscillators through optical trapping, *New J. Phys.* **14**, 045002 (2012).
- [26] T. Müller, C. Reinhardt, and J. C. Sankey, Enhanced optomechanical levitation of minimally supported dielectrics, *Phys. Rev. A* **91**, 053849 (2015).
- [27] A. Z. Barasheed, T. Müller, and J. C. Sankey, Optically defined mechanical geometry, *Phys. Rev. A* **93**, 053811 (2016).
- [28] K. K. Ni, R. Norte, D. J. Wilson, J. D. Hood, D. E. Chang, O. Painter, and H. J. Kimble, Enhancement of Mechanical q Factors by Optical Trapping, *Phys. Rev. Lett.* **108**, 214302 (2012).
- [29] N. Flowers-Jacobs, S. Hoch, J. C. Sankey, A. Kashkanova, A. M. Jayich, C. Deutsch, J. Reichel, and J. G. E. Harris, Fiber-cavity-based optomechanical device, *Appl. Phys. Lett.* **101**, 221109 (2012).
- [30] T. K. Paraiso, M. Kalaei, L. Zang, H. Pfeifer, F. Marquardt, and O. Painter, Position-Squared Coupling in a Tunable Photonic Crystal Optomechanical Cavity, *Phys. Rev. X* **5**, 041024 (2015).
- [31] I. S. Grudinin, H. Lee, O. Painter, and K. J. Vahala, Phonon Laser Action in a Tunable Two-Level System, *Phys. Rev. Lett.* **104**, 083901 (2010).
- [32] J. J. Viennot, X. Ma, and K. W. Lehnert, Phonon-Number-Sensitive Electromechanics, *Phys. Rev. Lett.* **121**, 183601 (2018).
- [33] X. Ma, J. J. Viennot, S. Kotler, J. D. Teufel, and K. W. Lehnert, Non-classical energy squeezing of a macroscopic mechanical oscillator, *Nat. Phys.* **17**, 322 (2021).
- [34] N. P. Bullier, A. Pontin, and P. F. Barker, Quadratic optomechanical cooling of a cavity-levitated nanosphere, *Phys. Rev. Research* **3**, L032022 (2021).
- [35] T. P. Purdy, D. W. C. Brooks, T. Botter, N. Brahm, Z. Y. Ma, and D. M. Stamper-Kurn, Tunable Cavity Optomechanics with Ultracold Atoms, *Phys. Rev. Lett.* **105**, 133602 (2010).
- [36] F. Elste, S. M. Girvin, and A. A. Clerk, Quantum Noise Interference and Backaction Cooling in Cavity Nanomechanics, *Phys. Rev. Lett.* **102**, 207209 (2009).
- [37] A. Sawadsky, H. Kaufer, R. M. Nia, S. P. Tarabrin, F. Y. Khalili, K. Hammerer, and R. Schnabel, Observation of Generalized Optomechanical Coupling and Cooling on Cavity Resonance, *Phys. Rev. Lett.* **114**, 043601 (2015).
- [38] T. Weiss and A. Nunnenkamp, Quantum limit of laser cooling in dispersively and dissipatively coupled optomechanical systems, *Phys. Rev. A* **88**, 023850 (2013).
- [39] T. Weiss, C. Bruder, and A. Nunnenkamp, Strong-coupling effects in dissipatively coupled optomechanical systems, *New J. Phys.* **15**, 045017 (2013).
- [40] D. Kilda and A. Nunnenkamp, Squeezed light and correlated photons from dissipatively coupled optomechanical systems, *J. Opt.* **18**, 014007 (2016).
- [41] K. Qu and G. S. Agarwal, Generating quadrature squeezed light with dissipative optomechanical coupling, *Phys. Rev. A* **91**, 063815 (2015).
- [42] W. J. Gu, G. X. Li, and Y. P. Yang, Generation of squeezed states in a movable mirror via dissipative optomechanical coupling, *Phys. Rev. A* **88**, 013835 (2013).
- [43] S. P. Vyatchanin and A. B. Matsko, Quantum speed meter based on dissipative coupling, *Phys. Rev. A* **93**, 063817 (2016).
- [44] Y. Yanay, J. C. Sankey, and A. A. Clerk, Quantum backaction and noise interference in asymmetric two-cavity optomechanical systems, *Phys. Rev. A* **93**, 063809 (2016).
- [45] R. Burgwal, J. del Pino, and E. Verhagen, Comparing nonlinear optomechanical coupling in membrane-in-the-middle and single-cavity systems, *New J. Phys.* **22**, 113006 (2020).
- [46] V. Dumont, S. Bernard, C. Reinhardt, A. Kato, M. Ruf, and J. Sankey, Flexure-tuned membrane-at-the-edge optomechanical system, *Opt. Express* **27**, 25731 (2019).
- [47] See Supplemental Material at <http://link.aps.org/supplemental/10.1103/PhysRevLett.129.063604> for more information, which includes Refs. [48–51].

- [48] M. Lawrence, B. Willke, M. Husman, E. Gustafson, and R. Byer, Dynamic response of a fabry-perot interferometer, *J. Opt. Soc. Am. B* **16**, 523 (1999).
- [49] D. Wilson, Cavity optomechanics with high-stress silicon nitride films, Ph.D. thesis, California Institute of Technology, 2011.
- [50] M. Rakhmanov, Dynamics of laser interferometric gravitational wave detectors, Ph.D. thesis, California Institute of Technology, 2000.
- [51] R. J. Lang and A. Yariv, Local-field rate equations for coupled optical resonators, *Phys. Rev. A* **34**, 2038 (1986).
- [52] The dependence of J on membrane displacement is neglected here, because its effect is much smaller than that of the other optomechanical couplings.
- [53] A. A. Clerk, M. H. Devoret, S. M. Girvin, F. Marquardt, and R. J. Schoelkopf, Introduction to quantum noise, measurement and amplification, *Rev. Mod. Phys.* **82**, 1155 (2010).
- [54] C. Stambaugh, H. Xu, U. Kemiktarak, J. Taylor, and J. Lawall, From membrane-in-the-middle to mirror-in-the-middle with a high-reflectivity sub-wavelength grating, *Ann. Phys. (Berlin)* **527**, 81 (2015).
- [55] G. Rempe, R. Lalezari, R. J. Thompson, and H. J. Kimble, Measurement of ultralow losses in an optical interferometer, *Opt. Lett.* **17**, 363 (1992).
- [56] H. R. Kong and K. S. Choi, Physical limits of ultra-high-finesse optical cavities: Taming two-level systems of glassy metal oxides, [arXiv:2109.01856](https://arxiv.org/abs/2109.01856).